Spectroscopic Measurements of Temperature and Plasma Impurity Concentration During Magnetic Reconnection at the Swarthmore Spheromak Experiment

Vernon H. Chaplin, Michael R. Brown, David H. Cohen, and Tim Gray
Department of Physics and Astronomy, Swarthmore College, Swarthmore, Pennsylvania 19081

Chris D. Cothran
Naval Research Laboratory, Washington, DC 20375 and
Department of Physics and Astronomy, Swarthmore College, Swarthmore, Pennsylvania 19081

Electron temperature measurements during counter-helicity spheromak merging studies at the Swarthmore Spheromak Experiment (SSX) [M. R. Brown, Phys. Plasmas **6**, 1717 (1999)] are presented. VUV monochromator measurements of impurity emission lines are compared with model spectra produced by the non-LTE excitation kinematics code PrismSPECT [J. J. MacFarlane *et al.*, in *Proc. of the Third Conf. on Inertial Fusion Science and Applications* (2004)] to yield the electron temperature in the plasma with 1 μs time resolution. Average T_e is seen to increase from 20 eV to $30-35$ eV during spheromak merging. Average C III ion energy, measured with a new ion Doppler spectrometer (IDS) [C. D. Cothran *et al.*, Rev. Sci. Instrum. **77**, 063504 (2006)], likewise rises during magnetic reconnection, also peaking at 30-35 eV, though this peak is earlier in time than the electron temperature peak. The VUV emission line measurements are also used to constrain the concentrations of various impurities in the SSX plasma, which are dominated by carbon, but include some oxygen and nitrogen. A comparison of time-dependent and steady state modeling results indicates that excitation and ionization equilibrium are achieved within several μs of spheromak formation, and therefore steady-state simulations of the plasma during reconnection are adequate to describe the spectral line formation. A burst of soft X-ray emission is seen during reconnection with a new four channel detector (SXR). Evidence is seen in the data for spectral changes in the soft X-ray emission as reconnection progresses, although our single-temperature equilibrium spectral models are not able to provide adequate fits to all the SXR data.

I. INTRODUCTION

Magnetic reconnection is the process driving the dynamics in spheromak merging and relaxation [1] as well as in several astrophysical scenarios [2]. During reconnection, magnetic energy is rapidly converted to electron and ion heat, plasma flow, and energetic particle beams [3, 4]. However, the partitioning of energy among various channels is not fully understood. Spheromak dynamics have been studied at the Swarthmore Spheromak Experiment (SSX) in a number of geometries [2, 5–8]. We have recently been studying spheromak merging in a prolate 0.4 m diameter, 0.6 m length, 3 mm wall copper flux conserver at SSX (see Fig. 1). In these experiments, merging of a pair of counter-helicity spheromaks generates magnetic reconnection dynamics near the midplane.

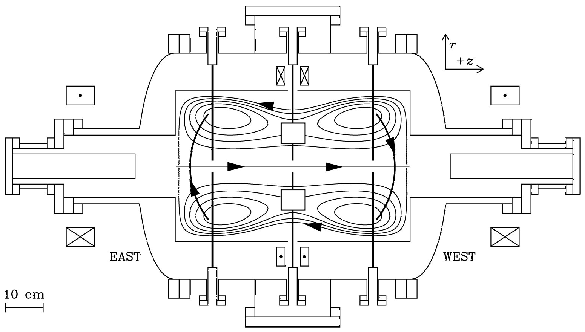

FIG. 1: Schematic of the SSX, shown in cross-section. The device is cylindrically symmetric about the horizontal axis in the figure. Spheromak plasmas are formed in the guns on the east and west sides of the vacuum chamber and ejected into the main flux conserver. The lines of sight of the VUV monochromator, the soft x-ray detector, and the ion Doppler spectrometer are at the midplane, aligned with the short axis of the chamber and perpendicular to the long axis, and here are indicated schematically by the white squares (see Fig. 9). Arrays of magnetic probes are shown schematically as six black lines in the figure. The probes are removed hen we take spectroscopic data. The contours represent the magnetic field lines of an FRC, the plasma structure that forms when two counter-helicity spheromaks merge.

Local and global magnetic structure of SSX spheromaks has been studied with up to 600 individual internal magnetic probes operated simultaneously at 1.25 MHz using a multiplexer system [9]. Line averaged electron density is monitored with a quadrature HeNe laser interferometer [3]. We can scan density in a range $n_e = 1 - 10 \times 10^{14}$ cm^{-3}, and find a typical value of $n_e = 5 \times 10^{14}$ cm^{-3}. The composition of the SSX plasma is primarily hydrogen, with trace concentrations of carbon and other impurities. The plasma is fully ionized and fully magnetized, with typical magnetic fields of 0.1 T and an ion gyroradius, $\rho_i \ll R$, where $R = 0.2$ m is the outer flux conserving boundary of the plasma (defined by a cylindrical copper wall). The Lundquist number S, the ratio of the resistive magnetic diffusion time τ_R to the Alfvén transit time τ_A, is large for SSX, $S \approx 1000$. Accordingly, the global structure of SSX spheromaks is fully in the magnetohydrodynamic (MHD)

regime ($S \gg 1, \rho_i \ll R$). Previous studies have constrained the plasma temperatures $T_e \approx T_i \leq 100$ eV [6, 10, 11].

Because magnetic reconnection is dynamically three-dimensional, it is often difficult to identify the reconnection site within the experimental volume or to determine whether the reconnection process has convected into the line of sight. In the experiments reported here, spectroscopic data are line-integrated over a 1 cm wide chord through a diameter at the midplane with a time resolution of about 1 μs. In addition, an ensemble of 20-30 discharges are typically averaged for each measurement.

Line averaged electron temperature and impurity concentration levels are inferred from model fits to data from a vacuum ultraviolet (VUV) spectrometer. Data are analyzed with a non-LTE excitation/ionization kinematics code. This modeling is also used to explore the extent to which time-dependent, non-equilibrium excitation and ionization has to be accounted for. Mean ion energy is measured with an ion Doppler spectrometer (IDS) [11].

In section II, details of the spectral modeling using the PrismSPECT code are presented. In section III, determinations of impurity concentration from the VUV spectrometer are presented. In section IV, we present measurements of the plasma electron temperature made using carbon emission line intensity ratios and compare these results with C III ion temperatures measured with IDS. In section V, we discuss the progress of additional electron temperature measurements utilizing model fits to data from a four-channel soft x-ray (SXR) array. A summary is presented in section VI.

II. SPECTRAL MODELING

A. PrismSPECT

We analyzed the SXR and VUV data using the PrismSPECT non-LTE excitation/ionization code [12, 13]. Simulations were run for spatially uniform plasmas with a variety of temperatures, densities, and compositions. Model spectra and line strength ratios from these simulations were compared to spectroscopic data from SSX to determine best fit values for the plasma parameters of interest. We also used time-dependent simulations to study the plasma's approach to ionization/excitation equilibrium after spheromak formation.

PrismSPECT models all significant radiative and collisional (including three-body) processes, though not charge exchange. In its time dependent mode, the code computes atomic level populations at each time step by integrating the relevant rate equations forward in time, and the calculated level populations and transition probabilities are used to produce a model spectrum. In the steady-state mode, equilibrium ionization balances and level populations are calculated by inverting a rate matrix. In both modes emissivities are calculated from the level populations and the emitted spectra are transported through the plasma taking optical depth effects into account. Doppler shifts from bulk motion are not accounted for in PrismSPECT, but all relevant line-broadening mechanisms – including the effects of natural, Stark, and thermal broadening – are accounted for [14]. This level of detail goes significantly beyond the coronal approximation, which we show below is necessary for accurate modeling of some of the emission lines we measure.

Atomic models for PrismSPECT simulations are drawn from the ATBASE database [15]. Many of the higher energy levels of impurity ions in the SSX plasma produce no strong spectral features, so we were able to make simplifications to the full ATBASE models and reduce simulation runtimes without sacrificing accuracy. Tests of a variety of atomic models revealed 200 energy levels per carbon ion and 50 levels per nitrogen ion to be sufficient, while the oxygen model used contained 50 levels for O III through O VII and one level for the other ions. Hydrogen in SSX is almost 100% ionized, and line radiation following recombination of protons and electrons was found to make only negligible contributions to SXR signals, so we used only the ground state of neutral hydrogen and ionized hydrogen in our atomic model for H. For each element, adding more levels per ion stage beyond these described above did not lead to any significant change in the calculated spectra.

B. Equilibration Time

The spheromak formation and expansion phases of an SSX discharge are characterized by turbulence and rapidly changing temperatures and densities [5]. Although it is difficult to estimate the time-varying conditions at the beginning of a discharge with a high degree of precision, the plasma conditions should not be varying significantly as the spheromaks approach the midplane. Here we investigate the extent to which the plasma is in ionization and excitation equilibrium. If it is, then the time history of the spheromak plasma is not important, and its spectrum can be modeled with a simple collisional-radiative equilibrium approach, in which the density, temperature, and composition are the only important parameters.

The experiments we report on here focus primarily on the merging of two spheromaks rather than on the spheromak formation process itself. The merging and associated reconnection generally occurs at about $t = 30$ to 40 μs and lasts for 20 to 30 μs, after which the plasma achieves a quasi-steady, relaxed configuration. The VUV monochromator and SXR view the plasma along fixed lines of sight through the midplane (see Fig. 1), so measured signals are typically zero for approximately the first 30 μs of a discharge and peak around $t = 50 - 60$ μs. Steady-state simulations will therefore be sufficient if they can accurately describe the conditions in the plasma at $t > 30$ μs.

To test this, we calculated the evolution of the excitation and ionization of a hydrogen plasma with trace levels of carbon, nitrogen, and oxygen for a set of assumed density and temperature values as a function of time, based on our estimates of the conditions before, during, and after spheromak formation. A variety of initial conditions were tested, with electron temperatures in the plasma gun ranging from 0.025 eV to 60 eV. The ion density used was 8×10^{15} cm^{-3} for the first 10 μs of the simulations (before the SSX plasma has left the gun), decreasing linearly to 5×10^{14} cm^{-3} during the following 20 μs (modeling the plasma's expansion into the main flux conserver). We computed ultraviolet spectra as well as quantities such as the mean charge state at many times during these simulations, and saw that these tended to approach a steady state after < 10 μs. We then compared the spectra at late times, between 30 and 40 μs, with spectra calculated assuming equilibrium conditions. Indeed, these late-time spectra are nearly identical.

We can explore this numerical result analytically. Using the expression for the collisional excitation cross section [16], we find the mean excitation time in SSX with $n_{\rm i} = 5 \times 10^{14}$ ions cm^{-3} and $T_{\rm e} = 30$ eV to be:

$$t \sim \frac{\sqrt{3kTm_e^3}}{n\pi\hbar^2} \sim 2 \times 10^{-7} \text{ s.} \qquad (1)$$

Therefore, in a period of several μs, each ion in SSX will be collisionally excited many times, indicating that equilibrium will be reached on a time scale (< 10 μs) that is short relative to the plasma lifetime, consistent with the results of the detailed simulations. Based on the observed insensitivity of late-time simulation results to initial conditions, tested for a range of initial temperatures and atomic level populations, we conclude that we can safely use steady-state simulations to model the VUV and SXR spectra.

C. Line Ratio Modeling

The SSX plasma, in the time leading up to reconnection, should be close to coronal equilibrium, in which all upward atomic transitions are assumed to be caused by collisions between ions and electrons, and all downward transitions are assumed to occur by spontaneous emission. Similarly, ionization is by electron impact and is assumed to be balanced by radiative recombination. Since collisional ionization and radiative recombination both scale with the square of the plasma density, the overall ionization balance in a coronal plasma is density independent, and the ratio of the intensities of two lines from different ionization stages of the same element can serve as an electron temperature diagnostic. The primary line ratio used for our temperature determinations was C III 97.7 nm / C IV 155 nm (hereafter written as $I_{97.7}/I_{155}$). Representative spectra, calculated for two different temperatures, are shown in Fig. 2, where these two carbon lines are prominent.

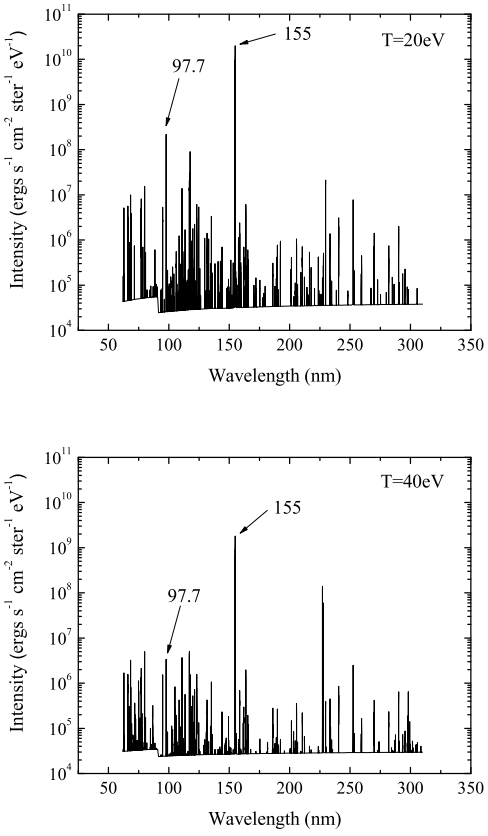

FIG. 2: Model spectra from steady-state simulations with $T_{\rm e}$ = 20 eV (top) and $T_{\rm e}$ = 40 eV (bottom). Both simulations assume a uniform 40 cm thick plasma composed of 99% hydrogen and 1% carbon with an ion density of 5×10^{14} cm^{-3}. The temperature dependence of the $I_{97.7}/I_{155}$ line ratio is evident. Note also the presence of the Lyman edge at 91.2 nm, indicating that radiative recombination of hydrogen, rather than bremsstrahlung, is the dominant continuum process at work.

Although the SSX plasma is close to coronal, we ran simulations that included the full range of atomic processes and found a noticeable density dependence in the $I_{97.7}/I_{155}$ ratio in the relevant density and temperature regimes, as shown in Fig. 3. Although the deviation from coronal equilibrium is slight, C III and C IV are subdominant ion stages at T $>$ 10 eV (see Fig. 4, where we show the temperature-dependent carbon ionization balance), so small absolute changes in their abundances can lead to large relative changes in the corresponding line intensity ratio. Because of this effect, it was necessary to obtain independent density measurements in order to use line ratios for precise calculations of electron temperature. We use an electron density value of $n_{\rm e} = 5 \times 10^{14}$ cm^{-3} based on measurements with the laser interferometer.

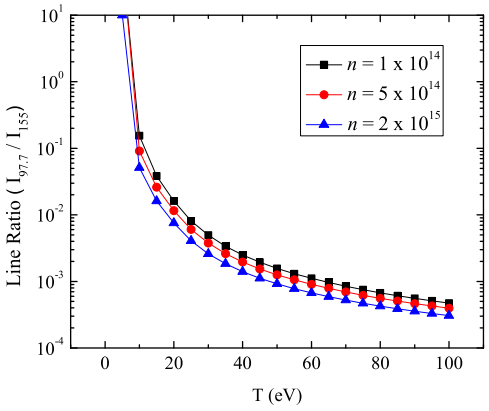

FIG. 3: Simulated $I_{97.7}/I_{155}$ line ratio plotted as a function of temperature for three different plasma densities (given in cm^{-3}). Note the mild density dependence of this line ratio.

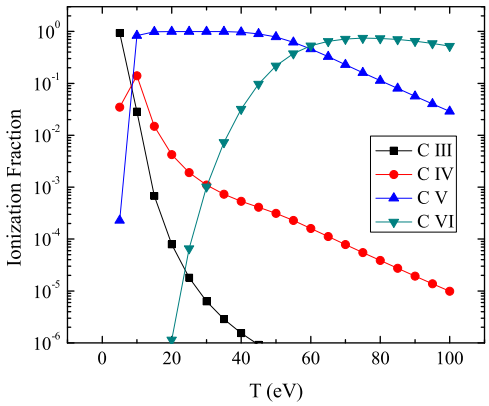

FIG. 4: Carbon ionization balance vs. electron temperature for an electron density of 5×10^{14} cm^{-3}.

III. IMPURITY DETERMINATIONS FROM VUV LINE MEASUREMENTS

Individual emission line strengths are measured in SSX using a vacuum ultraviolet (VUV) monochromator with a focal length of 0.2 m. Photons enter the device through a slit of adjustable width and strike a reflective diffraction grating, which selects and refocuses a narrow bandwidth around the desired central wavelength. Light leaving the diffraction grating is directed through an exit slit of adjustable width and into an 800 V photomultiplier tube (PMT). 500 μm was found to be the optimal exit slit width, corresponding to a spectral resolution of 2 nm. Signals from the PMT pass through a Stanford Research Systems SR570 current amplifier and are registered at

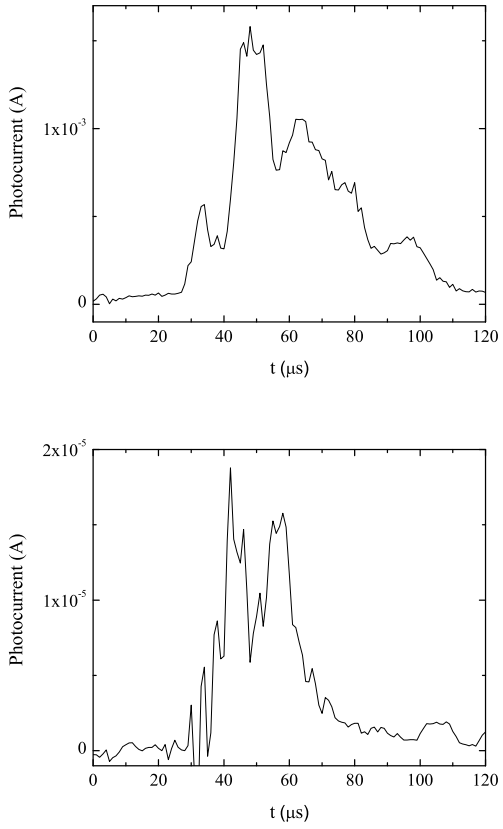

FIG. 5: Sample VUV monochromator data. Top: A measurement of the C IV 155 nm line intensity during a discharge with counter-helicity spheromak merging in SSX. Bottom: A measurement of the C III 97.7 nm line intensity during a single spheromak discharge.

10 ns intervals by an oscilloscope and transferred to a computer using LabView. Sample traces from individual discharges for two different lines are shown in Fig. 5.

PrismSPECT was used to identify the carbon, nitrogen, and oxygen lines most likely to be strong in SSX, and we tuned the monochromator to measure these lines. The results are summarized in Table I. Five emission lines produced signals that could be reliably distinguished from background noise: C III 97.7 nm, C IV 155 nm, C III 229.7 nm, N IV 124 nm, and O V 63.0 nm. The strongest of these was C IV 155 nm, which consistently produced PMT currents over 1 mA. C V is the dominant carbon ionization stage at SSX temperatures (see Fig. 4); however, being helium-like, its resonance lines arise in the K-shell, and so are outside the wavelength range accessible to the monochromator. Therefore it is not necessarily surprising that no C V lines were detected. The C V line at 227 nm is from a transition between two excited levels, and so is not expected to be extremely strong.

The comparative strengths of C, N, and O lines can yield information about the relative fractions of these im-

TABLE I: Impurity emission lines measured with the VUV monochromator.

Ion	λ (nm)	Transition	Typical Signal[a]
C III	97.7	$^1P_1 \rightarrow {}^1S_0$	10 μA
C IV	155	$^2P_{1/2,3/2} \rightarrow {}^2S_{1/2}$	1-2 mA
C V	227.4	$^3P_{0,1,2} \rightarrow {}^3S_1$	not detected
C III	229.7	$^1D_2 \rightarrow {}^1P_1$	10 μA
N IV	76.5	$^1P_1 \rightarrow {}^1S_0$	not detected
N V	124	$^2P_{1/2,3/2} \rightarrow {}^2S_{1/2}$	100 μA
O IV	55.4	$^2P_{1/2,3/2} \rightarrow {}^2P_{1/2,3/2}$	not detected
O V	63.0	$^1P_1 \rightarrow {}^1S_0$	5-10 μA
O VI	79	$^2D_{3/2,5/2} \rightarrow {}^2P_{3/2}$	not detected
O VI	103.5	$^2P_{1/2,3/2} \rightarrow {}^2S_{1/2}$	not detected

[a]Typical signals quoted are averaged over the 40-60 μs interval of each discharge.

purities present in SSX. These relative concentrations are a vital input for the simulations of soft x-ray spectra to be discussed in Section V. Of course, line ratios involving C, N, and O depend on temperature, the main parameter we are trying to constrain. Nevertheless, limits can be placed on relative impurity concentrations through comparisons of VUV line measurements with simulations.

We consider the ratios N V 124 nm / C IV 155 nm and O V 63.0 nm / C III 97.7 nm, in order to constrain the concentrations of N and O relative to C. We use the different carbon lines in order to minimize the temperature dependence of each diagnostic line ratio. As shown in Fig. 6, with equal concentrations of C, N, and O present, the simulated I_{124}/I_{155} ratio is $> 8/1$ for all plausible SSX plasma temperatures and about 20/1 for $T_e = 30$ eV. Yet, the measured intensity ratio is 1/15, implying a concentration of N that is roughly 300 times lower than that of C. Similar modeling for oxygen shows that the $I_{63.0}/I_{97.7}$ ratio is $> 970/1$ for all plausible SSX temperatures. However, measured strengths of the two lines are approximately equal, implying that carbon is ~ 1000 times more abundant than oxygen in SSX. The low concentrations of N and O are not surprising, as copper gasket seals are used on the SSX device and we employ an intensive program of high temperature bakeout and helium glow discharge conditioning before running the experiment.

Some insight into absolute impurity concentrations in the plasma can be garnered from an analogous analysis of the H I 121.6 nm / C III 97.7 nm line ratio, measured to be ~ 2 in SSX. Simulations with 99% H and 1% C predict a line ratio of 2 at 25-30 eV, so 1% carbon concentration is a reasonable estimate for SSX. However, the precision of this measurement is unclear because H I 121.6 nm (Lyman α) emission is only produced following proton-electron recombination and comes primarily from cool plasma near the flux conserver walls, while photons from the C III 97.7 nm transition are emitted throughout the plasma volume.

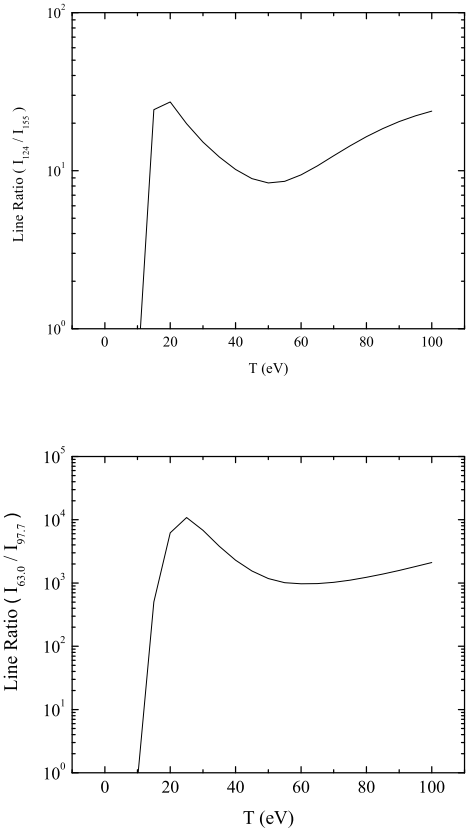

FIG. 6: Line ratios calculated from PrismSPECT simulations with 0.1% carbon, nitrogen, and oxygen impurities and $n_i = 5 \times 10^{14}$ cm^{-3}. The N V 124 nm line is predicted to be at least 8 times stronger than the C IV 155 nm line for plausible SSX temperatures (top), and the O V 63.0 nm line is predicted to be over 970 times stronger than the C III 97.7 nm line (bottom). The carbon lines are significantly stronger in the data than the nitrogen and oxygen lines, and those measurements, combined with the modeling shown here allow us to place an upper limit on the concentrations of nitrogen and oxygen relative to carbon in the SSX plasma.

IV. TEMPERATURE MEASUREMENTS

A. Electron Temperature

During the merging of two spheromaks, reconnection converts stored magnetic energy into thermal and kinetic energy. Understanding the details of this energy budget is vital for modeling coronal heating and other astrophysical phenomena. Electron temperatures during counter helicity spheromak merging were calculated by comparing measured and simulated (Fig. 3) values of the carbon line ratio $I_{97.7}/I_{155}$. Models show that even the strongest

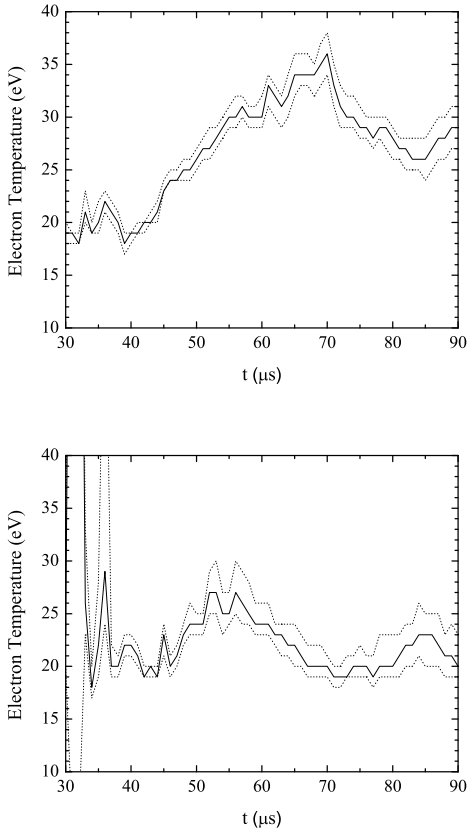

FIG. 7: Electron temperatures for counter helicity merging (top) and single spheromak discharges (bottom) derived from $I_{97.7}/I_{155}$ measurements averaged over 25 discharges for each line. An ion density of 5×10^{14} cm^{-3} was assumed. Dashed lines give the uncertainty range, defined as the temperatures implied by a line ratio one standard deviation above or below the mean.

emission lines in SSX are optically thin, so this comparison is quite straightforward. We determine an average electron temperature at each 1 μs bin from the ratio of the mean line intensities calculated from a set of 25 discharges for each line. The standard deviation of the line ratio at each time was used to define the uncertainty in the electron temperature. The results of the analysis of the $I_{97.7}/I_{155}$ ratio measurements are shown in Fig. 7.

The average electron temperature during counter helicity discharges increases from 20 eV to 35 eV during the $35 - 70$ μs time period (reconnection begins to occur by $t \sim 30 - 40$ μs), providing substantial evidence for magnetic energy being converted into heat. T_e rises rather gradually, however. A lesser temperature increase (~ 5 eV) is seen during single spheromak discharges, as the plasma relaxes into a lower-energy configuration around $t = 50$ μs. This measurement provides something of a control, indicating that the heating observed during reconnection is significant.

B. Ion Temperature

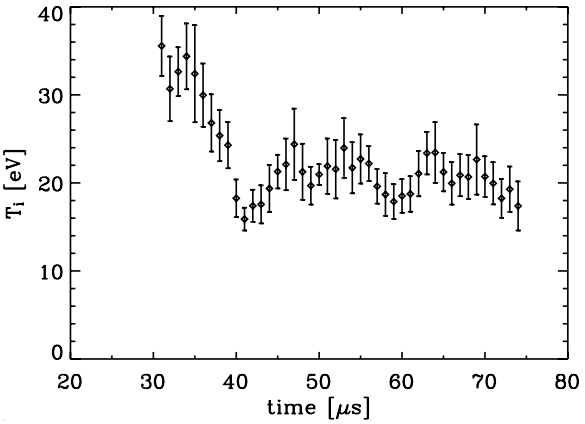

FIG. 8: Average ion temperature during counter helicity merging calculated from IDS measurements of the C III 229.7 nm line. These temperatures represent the mean of ten separate discharges during which the IDS view chord was along a diameter through the midplane. The measurement shown is a direct characterization of the line width, which we attribute completely to thermal broadening (after eliminating profiles with clearly non-thermal shapes). The data prior to ~ 30 μs, when the bulk of the plasma reaches the diagnostic line of sight and spheromak merging begins, is too noisy to be reliable.

Ion temperature and flow dynamics are monitored at the midplane of SSX with an ion Doppler spectrometer (IDS). The IDS instrument achieves high spectral resolution (0.0075 nm per pixel; equivalent to thermal broadening of carbon at a temperature of only 3 eV) and can measure the width and Doppler shift of impurity emission lines with 1 μs or better time resolution [11]. Non-thermal line profiles are sometimes seen, especially early in the reconnection process. The most obvious non-thermal profiles, which have double-peaked morphologies suggestive of bi-directional jets, have been removed from the datasets used in this analysis. However, some non-thermal contribution to the line widths may still be present, and so the quantity we derive from the measured line widths could perhaps be better characterized as a mean ion energy, rather than strictly a temperature. Fig. 8 shows the mean C III ion energy during counter helicity merging, derived from the second moment of the C III 229.7 nm lineshape data, averaged over ten discharges. Heating to 35 or 40 eV is seen as soon as reconnection is initiated, and subsequent cooling to roughly 20 eV is seen to occur around 40 μs, as the merging spheromaks begin to approach their relaxed, equilibrium configuration.

V. SXR MEASUREMENTS

The SSX soft x-ray detector (SXR) [6, 17–19], mounted at the mid-plane (see Fig. 9) and sampling a chord of

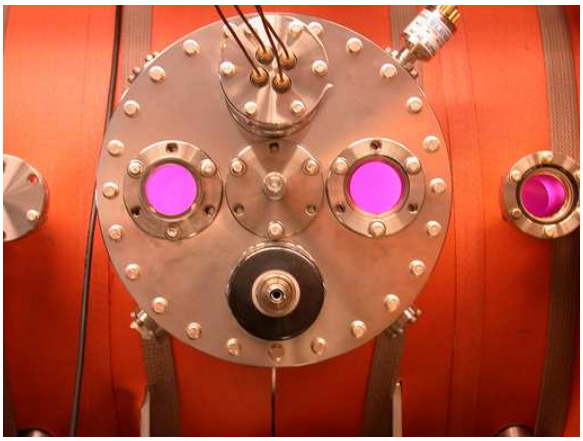

FIG. 9: Location of SXR at the midplane on the SSX machine (see the schematic in Fig. 1). The four wires at the top of the image carry current from the SXR photodiodes. Clockwise from upper left, the diodes are filtered by foils made of Al, Zr, Sn, and Ti. The port for the IDS is visible at the bottom center of this image. Note that hydrogen Balmer series recombination emission is visible through the windows in the vessel in this photograph.

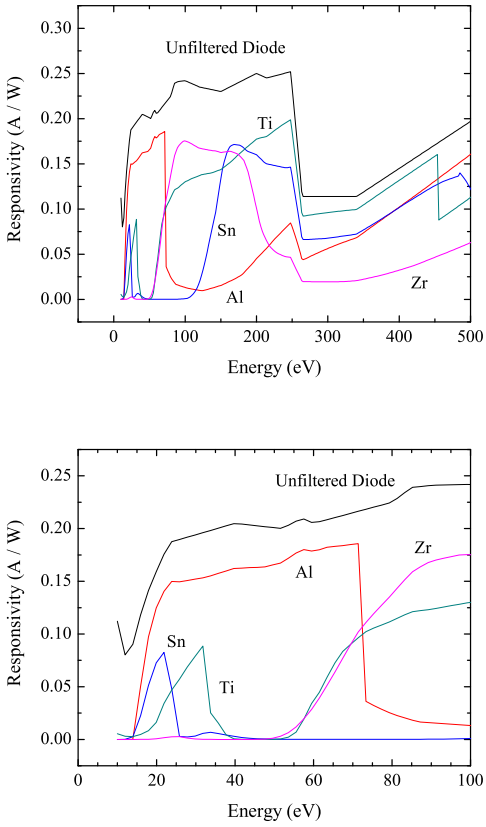

FIG. 10: SXR filter responsivities [20]. The colored lines show the response function of the filtered diodes in the 10 eV to 500 eV range, and the black line shows the response function of the unfiltered diode. Line emission at E > 500 eV was negligible at all simulation temperatures. The lower panel shows the same responsivity curves, but zoomed in on the range below 100 eV, where the bulk of the plasma emission is expected.

plasma in the reconnection region, measures the intensity of EUV and soft X-ray emission from the SSX plasma with a time resolution better than 10 ns. The SXR consists of a matched set of four International Radiation Detectors AXUV silicon p-n junction photodiodes filtered by thin films of aluminum (100 nm thick), titanium (50 nm), tin (100 nm), and zirconium (100 nm). The variation in the spectral response functions of the filters at EUV and soft x-ray energies, shown in Fig. 10, allows us to garner information not just about the time-dependent intensity of the soft X-ray emission, but also about broad spectral properties of the emission. Ultimately, we intend to use this data to supplement the VUV line ratio analysis and independently derive the electron temperature in SSX. Although the analysis of the SXR data lacks the simplicity of the line ratio measurement we make with the VUV monochrometer, it has the distinct advantage of allowing us to determine electron temperatures for individual discharges, since the flux through all four filters can be measured simultaneously. In addition, the SXR is sensitive to significantly higher energy photons than the VUV monochrometer, and thus can potentially measure emission from hotter plasma and even emission produced by a possible high-energy, non-Maxwellian component of the electron population.

In Fig. 11 we show the time-dependent soft X-ray signals measured in the four different SXR filters during one counter-helicity spheromak merging shot. X-ray emission is first detected when the plasma reaches the midplane at 25-30 μs and ramps up quite rapidly at 35-40 μs following the onset of magnetic reconnection. Intense emission is sustained for several tens of μs, with the relaxation to a merged, equilibrium configuration typically around 60 μs corresponding to a strong decrease in the SXR signal, as we expect for thermal emission arising from the heating associated with reconnection. We note that the signal in the Al bandpass is stronger than that seen in Ti or Zr, which is not surprising given the higher and broader spectral responsivity of the Al channel, shown in Fig. 10. The very strong Sn channel signal is quite unexpected, however, as the responsivity of this channel is not the highest at any photon energy. We verified that there is no low-energy leak (below 8 eV) by blocking this channel with UV fused silica and sapphire filters. However, there must be a problem with this channel, as there is no physical basis for the relative signal being this high, so we exclude the Sn channel data from the analysis we describe below.

In Fig. 12 we again show the SXR filter traces, but at an expanded scale afforded by the elimination of the Sn data. The time-dependence of each signal appears similar, but in the lower panel, where we show the time-

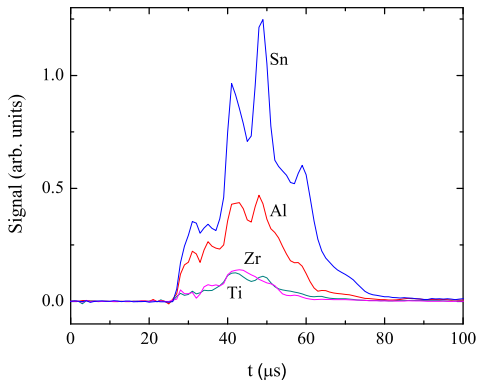

FIG. 11: Top: SXR data from a discharge with counter-helicity merging, smoothed over 1 μs intervals. Note the onset of strong soft X-ray emission around 30-40 μs, when reconnection begins.

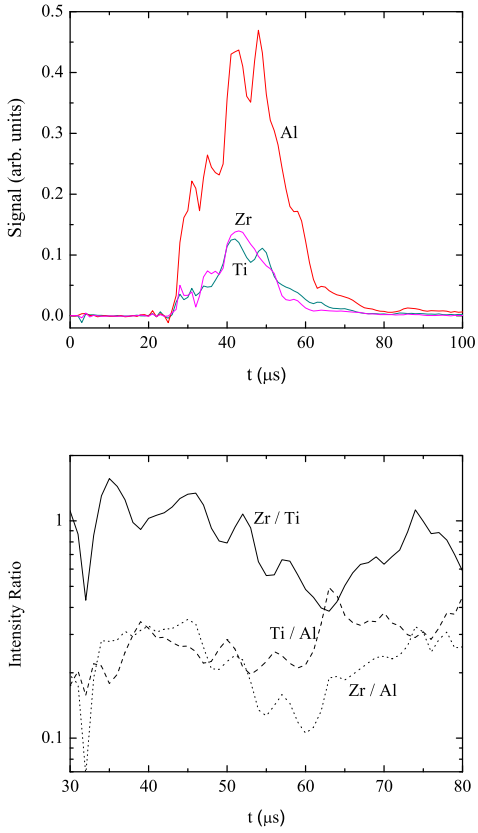

FIG. 12: Top: SXR data for the Al, Zr, and Ti filters from a discharge with counter-helicity merging, smoothed over 1 μs intervals. Bottom: Time evolution of filter ratios for the discharge. Sn filter data is omitted in order to more clearly show the time evolution of the other three ratios.

dependent channel intensity ratios, it is clear that the spectral signal of the X-ray emission changes in the interval 35 μs $< t <$ 60 μs. This is exactly the time frame of reconnection and relaxation toward a magnetic equilibrium that is seen in the magnetic data. The Ti/Al ratio is the most constant of the three during this time; the changes in the spectral energy distribution seem to be primarily due to the Zr signal. Looking at the response curves (Fig. 10), Zr has a significantly harder spectral response than Al and unlike Ti, has no significant response at low energies ($<$ 60 eV). Since the change seen in the channel intensity ratios with time (lower panel of Fig. 12) is in the sense of the Zr signal becoming weaker faster than the signal in the other two channels, this implies a spectral softening with time during reconnection.

We model the soft X-ray emission from the SSX plasma using the same type of PrismSPECT simulations we described earlier in the context of the VUV line ratio modeling. For the SXR analysis, we include C, N, and O in the ratios determined from the VUV line intensity measurements, and perform similar non-LTE, steady state simulations, calculating the emergent spectrum as a function of temperature at high resolution between 10 and 1000 eV. The absolute impurity concentrations (relative to hydrogen) are not important as long as the carbon concentration is above one part in 10^4, as our simulations show that the spectra are completely dominated by impurity line emission even at low concentration. A representative model spectrum is shown in Fig. 13. We multiply the temperature-dependent model soft X-ray spectra by the filter responsivities and integrate over photon energy to produce a model of the relative signal strength in each of the three (Zn, Al, Ti) channels. We then compare the measured intensity ratios from the three channels to the temperature-dependent model predictions. Note that by using ratios of the intensities we avoid errors due to our uncertain knowledge of the exact emissivity in the volume of plasma sampled by the SXR (which is affected by the detailed density distribution in the sampled volume, as well as the absolute impurity concentrations).

By comparing these model channel intensity ratios to the measured ratios in 1 μs intervals, we can, in principle, determine the time evolution of the electron temperature during a single discharge. The model-data comparison procedure for two time snapshots is shown in Fig. 14. What we find, however, is that there are times (as in the bottom panel in the figure) where no single temperature or small range of temperatures can explain all three intensity ratios. Perhaps the response at high energies is sensitive to some non-equilibrium physics that we do not include in our models. We have modeled the inclusion of Cu and other possible impurities, but thermal line emission from additional species does not appear to explain the discrepancies.

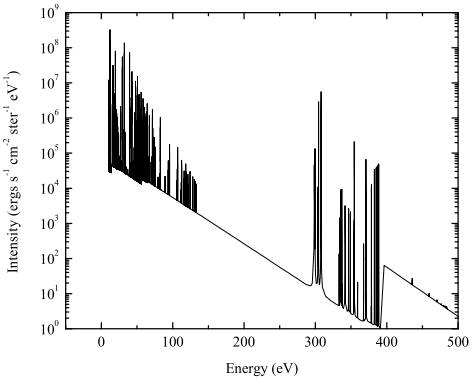

FIG. 13: Model spectrum from a steady-state simulation with $T_e = 30$ eV and $n_i = 5 \times 10^{14}$ cm^{-3}. Impurity concentrations of 1% carbon, 0.001% oxygen, and 0.0033% nitrogen were included. The plasma emits primarily at $E < 150$ eV, but SXR will also measure substantial emission from the C V and C VI resonance lines between 300 and 400 eV. Note that the Zr channel has the lowest responsivity at these energies, which is counter to what is seen below 100 eV.

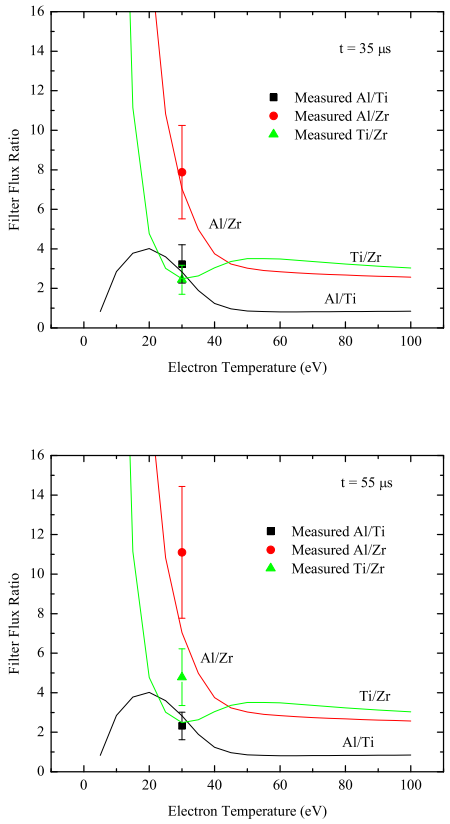

FIG. 14: Illustration of the process used to fit SXR data to model spectra and determine T_e. Channel intensity ratios calculated from models are plotted as a function of temperature (solid lines). Measured ratios at $t = 35$ μs (top panel) and $t = 55$ μs (bottom panel) during a typical single spheromak discharge are plotted as points at the location of the calculated best-fit temperature for the time step. For illustrative purposes, 30% error in the measured ratios is assumed. At $t = 35$ μs, a good fit is achieved at $T = 30$ eV. However, at $t = 55$ μs, all three measured ratios cannot match the models at any one temperature, and the best-fit temperature of 30 eV may not accurately reflect the actual T_e in the plasma.

VI. SUMMARY

We have shown that high time resolution UV spectroscopy is a useful tool for characterizing the physical properties of the SSX plasma during and after magnetic reconnection. Electron temperature can be estimated from impurity emission line ratios, but it is important to take into account deviations from coronal equilibrium, which requires detailed spectral modeling. This same modeling also shows that ionization and excitation equilibrium is reached within less than 10 μs after the plasma is discharged from the guns, so that steady-state simulations are sufficient for describing the plasma emission at the time that reconnection occurs (beginning 30 or 40 μs after the plasma discharge) and, furthermore, that the exact conditions in the plasma guns do not need to be known in order to accurately model the plasma properties around the time of reconnection.

Comparing model line ratios with measured UV line emission from various impurity species allows us to place constraints on the relative impurity concentrations in the plasma. Carbon is the dominant impurity in SSX, with a concentration approximately 300 times greater than that of nitrogen and 1000 times greater than that of oxygen. However, even the less abundant elements make a significant contribution to the UV and soft X-ray line emission.

For the first time in SSX we have made precise, high time resolution measurements of the electron temperature during counter helicity spheromak merging. Energy released by magnetic reconnection causes T_e to rise from approximately 20 eV to 35 eV on average during the 40 μs to 70 μs interval of a discharge. Average ion energies, as determined by line width measurements using an ion Doppler spectrometer also rise to roughly 35 eV, but much more rapidly; essentially as soon as reconnection begins. The delay in the electron heating may be an effect of the much greater mobility of electrons, compared to ions, and our sampling of a limited volume of the reconnecting plasma. In this case, the hot ions created thermally or non-thermally during reconnection stay within the centimeter-scale volume sampled by the IDS and VUV instruments, while the hot electrons, with their higher velocities, escape the region quickly (the mean free path of electrons at 20 eV is greater than the width of the sampling region). The electrons would have to be heated throughout the bulk of the SSX chamber before an appreciable signal in the carbon line ratios (or the SXR, presumably) could be seen.

Utilizing the information about impurity concentrations derived from UV line intensity measurements, we have developed a framework for monitoring electron temperature during individual discharges using a broadband soft x-ray detector, and the same spectral modeling tools that we used successfully to model the UV emission lines. The soft X-ray signal measured by the SXR increases dramatically during reconnection, and also shows a modest change in its spectral energy distribution. However, our steady-state non-LTE models (which assume statistical equilibrium in the excitation/ionization state of the plasma) cannot reliably reproduce the time evolution of the SXR signals, indicating that additional physics – for example, non-Maxwellian particle distributions – must be included in future modeling.

Acknowledgments

The authors gratefully acknowledge the technical assistance of S. Palmer and J. Haldeman at Swarthmore, and J. MacFarlane at Prism Computational Sciences, as well as some preliminary modeling done by V. Swisher at Swarthmore. This work was supported by DOE grant ER54604, by the NSF Center for Magnetic Self-Organization, and by a Eugene M. Lang summer research fellowship from the Provost's Office at Swarthmore College.

References

[1]M. R. Brown, Phys. Plasmas **6**, 1717 (1999).

[2]M. R. Brown, C. D. Cothran, and J. Fung, Phys. Plasmas **13**, 056503 (2006).

[3]M. R. Brown, C. D. Cothran, M. Landreman, D. Schlossberg, W. H. Matthaeus, G. Qin, V. S. Lukin, and T. Gray, Phys. Plasmas **9**, 2077 (2002).

[4]M. R. Brown, C. D. Cothran, M. Landreman, D. Schlossberg, W. H. Matthaeus, G. Qin, V. S. Lukin, and T. Gray, Astroph. Journal Lett. **577**, L63 (2002).

[5]C. G. R. Geddes, T. W. Kornack, and M. R. Brown, Phys. Plasmas **5**, 1027 (1998).

[6]C. D. Cothran, A. Falk, A. Fefferman, M. Landreman, and M. R. Brown, Phys. Plasmas **10**, 1748 (2003).

[7]C. D. Cothran, M. Landreman, M. R. Brown, and W. H. Matthaeus, Geophys. Res. Lett. **32**, L03105 (2005).

[8]M. R. Brown, C. D. Cothran, J. Fung, M. Chang, J. Horwitz, M. J. Schaffer, J. Leuer, and E. V. Belova, Phys. Plasmas **13**, 102503 (2006).

[9]M. Landreman, C. D. Cothran, M. R. Brown, M. Kostora, and J. T. Slough, Rev. Sci. Instrum. **74**, 2361 (2003).

[10]M. R. Brown, C. D. Cothran, D. H. Cohen, J. Horwitz, and V. Chaplin, **27**, 16 (2008).

[11]C. D. Cothran, J. Fung, M. R. Brown, and M. J. Schaffer, Rev. Sci. Instrum. **77**, 063504 (2006).

[12]Prism Computational Sciences, Inc., *PrismSPECT*, Spectral Analysis Code, www.prism-cs.com/Software/PrismSPECT/PrismSPECT.htm.

[13]J. J. MacFarlane, I. E. Golovkin, P. R. Woodruff, D. R. Welch, B. V. Oliver, T. A. Mehlhorn, and R. B. Campbell, in *Proceedings of the Third Conference on Inertial Fusion Science and Applications, Monterey, California*, edited by B. A. Hammel, D. D. Meyerhofer, J. M. ter Vehn, and H. Azechi (Am. Nuc. Soc., 2004).

[14]I. E. Golovkin, J. J. MacFarlane, P. Woodruff, J. E. Bailey, G. Rochau, K. Peterson, T. A. Mehlhorn, and R. C. Mancini, J. Quant. Spect. Rad. Transfer **99**, 199 (2006).

[15]Prism Computational Sciences, Inc., *Prism atomic physics data*, Prism Atomic Data, www.prism-cs.com/Software/AtomicData/AtomicData.htm.

[16]D. E. Osterbrock, *Astrophysics of Gaseous Nebulae and Active Galactic Nuclei* (University Science Books, Mill Valley, CA, 1989).

[17]J. F. Hansen, Ph.D. thesis, Caltech (2001).

[18]S. Hokin, R. Fonck, and P. Martin, Rev. Sci. Instruments **63** (1992).

[19]V. A. Soukhanovskii, D. Stutman, M. Iovea, M. Finkenthal, H. W. Moos, T. Munsat, B. Jones, D. Hoffman, R. Kaita, and R. Majeski, Rev. Sci. Instrum. **72** (2001).

[20]Lawrence Berkeley National Laboratory, *Filter transmission*, *X-Ray Interactions with Matter*, http://henke.lbl.gov/optical_constants/filter2.html.